Applied Ocean Research 63 (2017) 129–141

Contents lists available at ScienceDirect

Applied Ocean Research

journal homepage: www.elsevier.com/locate/apor

Neumann-Michell theory-based multi-objective optimization of hull form for a naval surface combatant

Jianwei Wu, Xiaoyi Liu, Min Zhao*, Decheng Wan

State Key Laboratory of Ocean Engineering, School of Naval Architecture, Ocean and Civil Engineering, Shanghai Jiao Tong University, Collaborative Innovation Center for Advanced Ship and Deep-Sea Exploration, Shanghai 200240, China

ARTICLE INFO

Article history:
Received 19 May 2016
Received in revised form
19 December 2016
Accepted 4 January 2017
Available online 19 January 2017

Keywords:
OPTShip-SJTU
Multi-objective optimization
NSGA-II algorithm
Neumann-Michell theory
Wave drag

ABSTRACT

A numerical multi-objective optimization procedure is proposed here to describe the development and application of a practical hydrodynamic optimization tool, OPTShip-SJTU. Three components including hull form modification module, hydrodynamic performance evaluation module and optimization module consist of this tool. The free-form deformation (FFD) method and shifting method are utilized as parametric hull surface modification techniques to generate a series of realistic hull forms subjected to geometric constraints, and the Neumann-Michell (NM) theory is implemented to predict the wave drag. Moreover, NSGA-II, a muti-objective genetic algorithm, is adopted to produce pareto-optimal front, and kriging model is used for predicting the total resistance during the optimization process to reduce the computational cost. Additionally, the analysis of variance (ANOVA) method is introduced to represent the influence of each design variable on the objective functions. In present work, a surface combatant DTMB Model 5415 is used as the initial design, and optimal solutions with obvious drag reductions at specific speeds are obtained. Eventually, three of optimal hulls are analyzed by NM theory and a RANS-based CFD solver naoe-FOAM-SJTU respectively. Numerical results confirm the availability and reliability of this multi-objective optimization tool.

1. Introduction

At present, hydrodynamic optimization of hull forms has gained extensive attention due to the considerable benefits associated with ship design. Hydrodynamic performances are enhanced through the optimization process, so the optimal ship will become more energy-saving and competitive. In the past, ship designers had to try a large number of combinations of design variables to search for the optimal solution by experimental tests, but it is considered to be too expensive, inefficient and less accurate. With the development of computer techniques, the advanced simulation analysis methods, geometrical modification methods and optimization algorithms are integrated in various ship hydrodynamic optimization tools.

Successful hull form optimization requires an efficient and flexible technique to represent and modify the hull geometry. Some researchers have attempted to deal with this problem. Kim [1] modified the Wigley hull form basing on parametric hull representation and NURBS surface, and Peri et al. [2] utilized Bézier Patch to complete the modification of hull geometry, while the FFD method was employed by Tahara et al. [3] to modify the shape of Delft Catamaran. For the sake of simplicity and flexibility, two ideal approaches including shifting method and FFD method are utilized in present study.

Automatic evaluation of hydrodynamic performance for each alternative hull form is an important part during the optimization process. Both of the potential flow theory and advanced RANS-based CFD method had been employed to predict the hydrodynamic performance during the hull optimization. For example, Suzuki et al. [4] used potential flow solver based on Hess and Smith method [5] and Rankine source method [6] to evaluate the energy of secondary flow for a tanker hull form optimization. Zhang [7] obtained the optimized hull form with minimum wave-making based on Ranking source method. Percival et al. [8] presented a method to minimize the total calm-water drags with a simple way to modify the ship hull forms, and the friction drag was estimated using the classical ITTC formula, and the wave drag was predicted using the zero-order slender-ship approximation. The results confirmed that this simple way could be useful enough for routine practical application to hull form optimization with the extreme simple drag prediction method. Campana et al. [9] and Tahara et al. [10] adopted two free-surface RANS solvers to

* Corresponding author.
E-mail address: min.zhao@sjtu.edu.cn (M. Zhao).

http://dx.doi.org/10.1016/j.apor.2017.01.007
0141-1187/

predict the total resistances in different simulation-based design (SBD) approaches. Compared between potential flow theory and RANS method for ship hydrodynamic prediction, RANS method requires several hours while potential flow theory requires several only a few minutes or even seconds [11]. Kim [1] pointed out that potential flow assumptions were suitable for preliminary and early hydrodynamic design with respect to efficiency and robustness. Nobless et al. [12] presented an efficient potential theory, Neumann-Michell (NM) theory, which yielded more realistic predictions of wave profiles and wave drag than the Hogner slender-ship approximation, at no appreciable increase in computational cost (seconds on a PC) for the classical Wigley parabolic hull. Besides, there are a lots of research about comparisons of experimental measurements of wave drag with numerical predictions obtained using a preliminary version of the NM theory for the Wigley hull, the Series 60 and DTMB 5415 model. Yang and Huang [13] presented that the sum of the ITTC friction drag and the Neumann-Michell (NM) theory wave drag could be expected to yield realistic practical estimates, which could be useful for routine applications to design and ship hull form optimization of a broad range of displacement ships. The computation of the steady flow around a moving ship based on NM theory is efficient and robust due to the succinctness of this theory, and Kim et al. [14] pointed that the wave drag predicted by NM theory is in fairly good agreement with experimental measurements. Therefore, NM theory is integrated in the optimization process to evaluate the objective functions for ship hydrodynamics.

However, a large number of alternatives should be evaluated during the optimization process, so the performance evaluation tool has to be called repeatedly, and this process will lead to large computation cost inevitably. Various methods have been proposed to deal with this challenge. Diez et al. [15] presented Karhunen–Loève Expansion (KLE) to reduce the dimension of design spaces during the hull form optimization, while a desired level of geometric variance could be defined by users on the basis of a trade-off between geometric variance and acceptable computational cost. Establishing the approximation model as a surrogate is also an efficient way to reduce calculation burden, and the design of experiments (DOE) methods are always utilized to generated appropriate samples for the approximation model. Tahara et al. [10] applied an orthogonal array to obtain the sample points, and the radial basis function network (RBFN) was used to established the approximation model of simulation analysis. Kim et al. [16] used kriging model combined with Latin hypercube sample (LHS) method to construct approximation model. In this work, kriging model are chosen for constructing the approximation model due to its flexibility and accuracy. This method developed from the field of geo-statistics has showed excellent performance in approximating both of linear and nonlinear functions, and is becoming widely used in engineering field. Besides, a modified Latin hypercube design method called optimized Latin hypercube sampling (OLHS) method is applied here to generate the DOE design matrix which satisfies the requirements of orthogonality and uniformity, thus, the computation cost of the optimization task decreases remarkably.

The selection of an appropriate optimization scheme is critical to obtaining the optimal solutions. Various algorithms have been investigated and compared [16–19]. Indeed, global optimization algorithms are obviously better suited to handle the typical hull form optimization problems, because the local optimization schemes are easily trapped in the local optimum and appeared premature convergence. Furthermore, single-objective optimization design always leads to the poor results that a large drag reduction is only obtained at a certain speed while a sharp drag increase may be detected in off-design speed ranges. Therefore, a multi-objective optimization scheme should be adopted, and then the optimal ship hulls will have a consistent drag reduction in a large range of speed compared with the initial one. Here, the multi-objective genetic algorithm named Non-dominated Sorting Genetic Algorithm (NSGA)-II has been employed to provide pareto-optimal front.

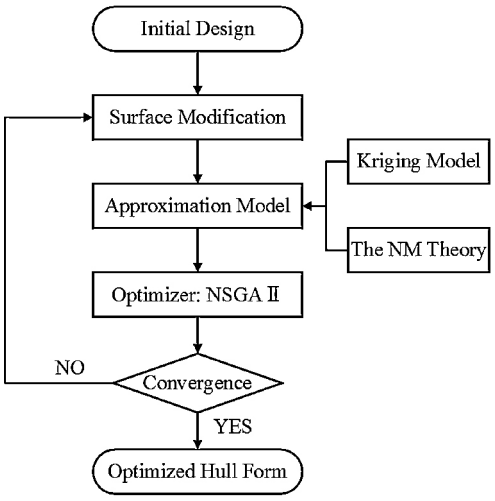

Fig. 1. The flow chart of the iterative optimization process.

In this paper, a surface combatant DTMB Model 5415 is adopted as the initial hull form, and the geometry of hull form is modified globally and locally by shifting method and FFD method respectively. The Kriging model is established based on the samples produced by OLHS method and is used to provide the drag prediction in optimization process. The ANOVA test is also carried out to represent the influence of each design variable on the objective functions. Eventually, the optimal hull forms with obvious drag reductions are obtained by using NSGA-II algorithm and are verified by NM theory and a RANS-based CFD solver naoe-FOAM-SJTU, which is developed under the framework of the open source code, OpenFOAM, and has been validated in RANS computations of a ship with heave and pitch motions in head waves [20]. The flow chart of the iterative optimization process is illustrated in Fig. 1.

2. Modification of hull geometry

Appropriate and effective surface modification methods are critical to optimization process. On the one hand, these techniques should modify hull forms efficiently and ensure the rationality of the new hull surface, on the other hand, the number of variables involved in these methods should keep as low as possible—too

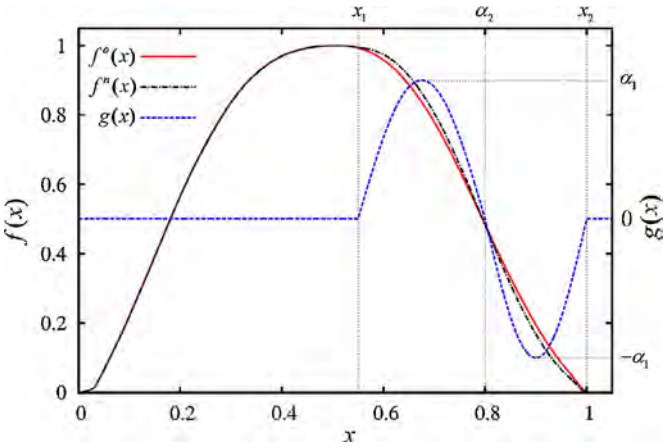

Fig. 2. An application of shape function g to modify the sectional area curve.

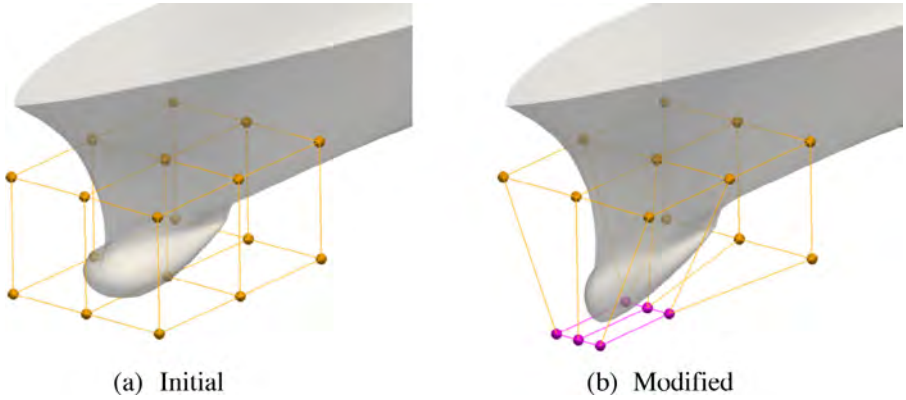

Fig. 3. An application of FFD method to modify the ship bow.

much design variables will increases the complexity of the problem and lead to vast computational cost. In this paper, two approaches, shifting method [16] and FFD method [21], are employed to modify the geometry of hull form globally and locally respectively, and the former is used to modify the sectional area curve of the hull while the latter is to deform a solid geometric model based on trivariate Bernstein polynomials. The combination of the two approaches makes the deformation more flexible and only a few design variables involved.

2.1. Shifting method

In shifting method, hull forms are represented by using the sectional area curves. A new hull shape can be derived by adjusting the longitudinal spacing of the transverse sections to suit the new curve of sectional area, which is obtained by modifying the initial one through a shape function.

The expression of the new sectional area curve is developed as follows:

$$f^n(x) = f^0(x) + g(x, \alpha_1, \alpha_2) \tag{1}$$

where the shape function g is defined as:

$$g(x) = \begin{cases} \alpha_1 \left[0.5(1 - \cos 2\pi \dfrac{x - \alpha_2}{\alpha_2 - x_1}\right]^{0.5}, x_1 \le x \le \alpha_2 \\ -\alpha_1 \left[0.5(1 - \cos 2\pi \dfrac{x - \alpha_2}{\alpha_2 - x_2}\right]^{0.5}, \alpha_2 \le x \le x_2 \\ 0, \textit{elsewhere} \end{cases} \tag{2}$$

in which $f^n(x)$ represents the expression of new sectional area curve while $f^0(x)$is corresponding to the initial one; $g(x)$ is the shape function with four arguments; x_1 and x_2 control the range of area needed to be modified; α_1 determines the slope of the new sectional area curve, and α_2 denotes the location of the fixed station. An application of shape function g is carried out and the initial curve of sectional area is modified partly. All of these are illustrated in Fig. 2.

Obviously, once the four parameters are determined, new sectional area curve and corresponding hull shape will be obtained. Various hull forms can be derived during the optimization process by changing the values of these four arguments, and the unrealistic hulls with unreasonable oscillations of the new sectional area curve can be avoided due to the simple form of shape function g. Detailed application of this method can be founded in [16].

In present study, since hull surface is discretized by triangle elements, a new hull form can be obtained just by moving the grid nodes, and the amount of movement is determined by the difference between the new and original sectional area curves.

2.2. Free form deformation (FFD)

The surface shape around the ship bow is critical to the resistance performance, so it is necessary to employ a method to modify the local hull surface, especially the shape of ship bow.

FFD technique, proposed by Sederberg and Parry [21] based on trivariate Bernstein polynomials, is utilized to perform the deformation of solid geometric models in a free-form manner. In this method, the objects to be deformed are embedded into a plastic parallelepiped, and then these objects are deformed along with it. The modification of hull form is defined and controlled by using a few control nodes, and the displacements of them are utilized as design variables by optimizer.

In present study, FFD technique is utilized as a local modification tool for the stem profile. Surface near the ship bow is embedded into a parallelepiped in which the control points are imposed. Firstly, the local coordinates of each node on initial bow surface are computed. Then, some of control points are moved to the new positions in terms of the design variables determined by specific optimization algorithm. Finally, the new locations of every node on bow surface are evaluated. Thus, the modified bow surface is obtained while the hull surface outside of the parallelepiped still remains unchanged. This method was also adopted in Tahara et al. [17] and Peri et al. [22]. More details about the scheme can be found in [21].

An application of FFD approach to modify a ship bow was shown in Fig. 3. The surface to be deformed is wrapped by a parallelepiped, and both of the movable control points (purple spheres) and fixed control points (yellow spheres) are shown. Significant differences due to the movements of control points can be observed between the two bow shapes shown in Fig. 3(a) and Fig. 3(b).

3. Introduction of Neumann-Michell theory

A practical simulation tool is one of the main components for hull form optimization procedure. The optimizer is guided by the evaluating results involved thousands of alternatives toward the improved solutions, accordingly, both accuracy and efficiency are important for this tool.

In this study, Neumann-Michell (NM) theory [11] is employed to evaluate the drag of a ship hull. This theory can yield realistic predictions of wave drags at low computational cost. Due to the simplicity and fast computation, the similar potential theory has been used for hull-form optimization [23,24].

3.1. Brief introduction of Neumann-Michell theory

When a ship steadily advances at constant speed along a straight path in calm water of effectively infinite depth and lateral extent,

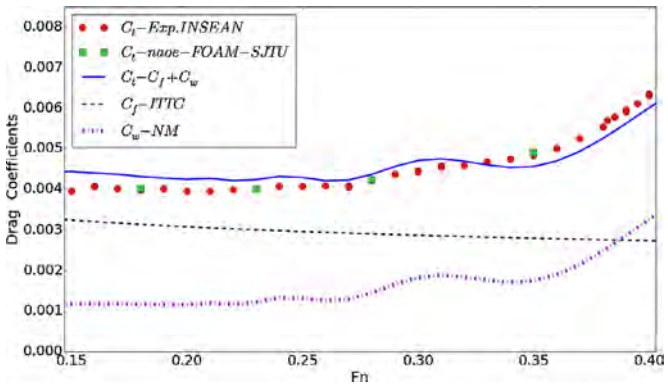

Fig. 4. Comparison of drag coefficients for the DTMB Model 5415.

the wave drag related to the waves generated by the advancing ship hull is of considerable practical importance because drag is a critical and dominant hydrodynamic factor for ship design. The Neumann–Michell (NM) theory is an efficient potential flow theory used to predict the ship waves. In this theory, both of the surface tension and the free surface nonlinearities are ignored for the practical goal, and the viscosity effect is estimated by considering the turbulent viscous boundary layer on a flat plate. This theory is the modification of Neumann-Kelvin theory and based on a consistent linear flow model. The main difference between the two theories is that the line integral around the ship waterline that occurs in the classical NK boundary-integral flow representation is eliminated in the NM theory, so the NM theory expresses the flow about a steadily advancing ship hull in terms of a surface integral over the ship hull surface. The Neumann-Michell potential representation is expressed as below, and more details of this theory can be found in Ref [12].

$$\tilde{\varphi} \approx \tilde{\varphi}_H + \tilde{\psi}^W \tag{3}$$

where the two components are defined as:

$$\tilde{\varphi}_H = \int_{\sum}^{H} Gn^x da - \int_{\sum}^{F} G\pi^{\varphi} dxdy \tag{4a}$$

$$\tilde{\psi}^W = \int_{\sum}^{H} (\varphi_{t'} \mathbf{d}_* + \varphi_{d'} \mathbf{t}_*) \cdot \mathbf{W} da \tag{4b}$$

3.2. Validation of the Neumann-Michell solver

The validation study for NM theory is carried out before the optimization. For DTMB Model 5415, the comparisons between experimental data and drag predictions given by NM theory (C_w), ITTC formula (C_f), and naoe-FOAM-SJTU are shown in Fig. 4.

It can be seen from Fig. 4 that the drag coefficients predicted by NM and ITTC formula are in consistent agreement with the experimental measurements [25], and NM theory can provide correct relative comparisons of the drags of alternative solutions despite the results related to NM are not as accurate as that of naoe-FOAM-SJTU. Besides, NM theory requires only a few minutes using a PC to obtain the prediction while naoe-FOAM-SJTU requires several hours or even days, so the efficiency of NM theory is higher than naoe-FOAM-SJTU, which is much more critical to optimization at early stage. Therefore, this practical prediction method based on NM theory is quite qualified for the optimization work.

4. Optimization module

Optimization module plays an important role in the optimization tool. The aim of this module is to minimize objective functions during the optimization process. In present study, a muti-objective genetic algorithm, called NSGA-II, is adopted to obtain the pareto-optimal front. However, the computation associated with global optimal algorithm and simulation codes is very expensive, so a statistical approximation model with DOE method is employed to reduce the computational cost.

4.1. Design of experiment

Constructing approximation model (or metamodels) based on computer experiments is becoming widely used in engineering to reduce the computational cost. In order to improve the space-filling property and computational efficiency in sampling, various design methods has been proposed, such as factorial design [26], Latin hypercube design (LHD) [27], etc.

In this work, optimal Latin hypercube sample method [28], a modified Latin hypercube design, is used for sampling. An application of optimal Latin hypercube design with two factors and nine design points is illustrated in Fig. 5. Fig. 5(a) shows the standard orthogonal array and Fig. 5(b) shows the random Latin hypercube design matrix. In Fig. 5(c), the optimal Latin hypercube design matrix is displayed, and the design points cover all levels of each factor as well as spread evenly within the design space.

4.2. Mathematics of kriging model

Kriging model [26,27] is developed from mining and geostatistical applications involving spatially and temporally correlated data. This model combines a global model and a local component:

$$y(x) = f(x) + z(x) \tag{5}$$

where $y(x)$ is the unknown function of interest,$f(x)$ is a known approximation function of$x$, and$z(x)$ is the realization of a stochastic process with mean zero, variance $\hat{\sigma}^2$, and non-zero covariance.

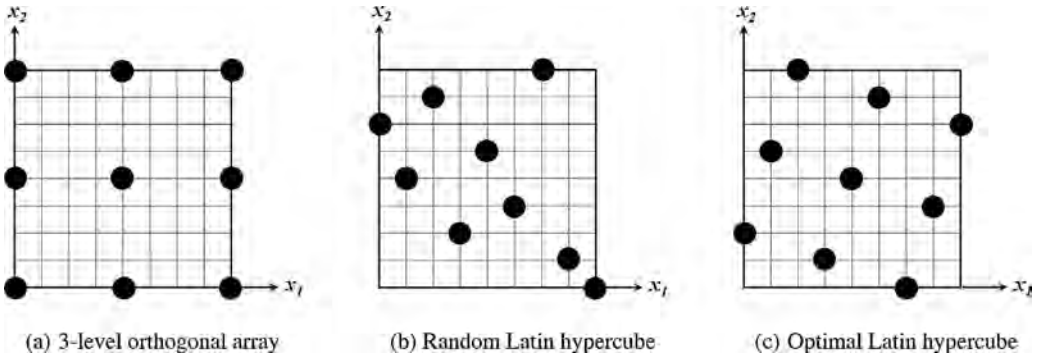

Fig. 5. Three types of experimental design method [29].

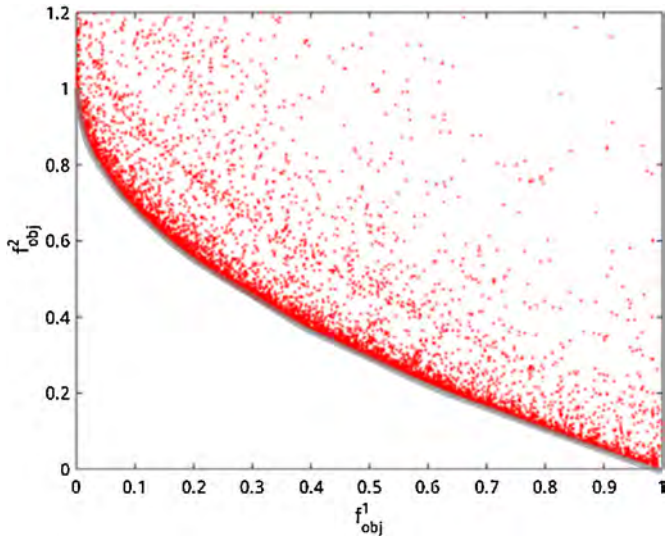

Fig. 6. Pareto Front and individuals for test function generated by NSGA-II.

Fig. 7. The geometry of DTMB Model 5415.

The kriging predictor is given by:

$$\hat{y} = \hat{\beta} + \boldsymbol{r}^T(x)\boldsymbol{R}^{-1}\left(\boldsymbol{y} - \boldsymbol{f}\hat{\beta}\right) \tag{6}$$

where $\boldsymbol{y}$ is an n_s-dimensional vector that contains the sample values of the response; $\boldsymbol{R}$ is the correlation matrix; $\boldsymbol{f}$ is a column vector of length n_s that is filled with ones when $\boldsymbol{f}$ is taken as a constant; $\boldsymbol{r}^T(x)$ is the correlation vector of length n_s between an untried x and the sampled data points $\{x^{(1)}, x^{(2)}, \ldots, x^{(ns)}\}$ and is expressed as:

$$\mathbf{r}^{\mathrm{T}}(x) = \left[R\left(x, x^{(1)}\right), R\left(x, x^{(2)}\right), \ldots, R\left(x, x^{(n_s)}\right)\right]^T \tag{7}$$

Additionally, the Gaussian correlation function is employed in this work:

$$R\left(x^i, x^j\right) = exp\left[-\sum_{k=1}^{n_{dv}} \theta_k \left|x_k^i - x_k^j\right|^2\right] \tag{8}$$

In Eq. (6), $\hat{\beta}$. is estimated as:

$$\hat{\beta} = \left(\boldsymbol{f}^T\boldsymbol{R}^{-1}\boldsymbol{f}\right)^{-1}\boldsymbol{f}^T\boldsymbol{R}^{-1}\boldsymbol{y}. \tag{9}$$

The estimate of the variance$\hat{\sigma}^2$, between the underlying global model $\hat{\beta}$ and $\boldsymbol{y}$ is estimated using Eq. (10):

$$\hat{\sigma}^2 = \left[\left(y - \boldsymbol{f}\hat{\beta}\right)^T \mathrm{R}^{-1}\left(y - \boldsymbol{f}\hat{\beta}\right)\right]/ns \tag{10}$$

where $f(x)$ is assumed to be the constant $\hat{\beta}$. The maximum likelihood estimates for the θ_k in Eq. (8) used to fit a kriging model are obtained by solving Eq. (11):

$$\max_{\theta_k > 0} \Phi\left(\theta_k\right) = -\left[n_s \ln\left(\hat{\sigma}^2\right) + ln|\boldsymbol{R}|\right]/2 \tag{11}$$

where both $\hat{\sigma}^2$ and $|\boldsymbol{R}|$ are functions ofθ_k. While any value for the θ_k creates an interpolative kriging model, the "best" kriging model is found by solving the k-dimensional unconstrained, nonlinear, optimization problem given by Eq. (11).

In the end, it is notable that the CPU time consumed in the present optimization procedure is only a few minutes (1–2 min) on a PC. This fact proves the high efficiency of the optimization based on kriging model.

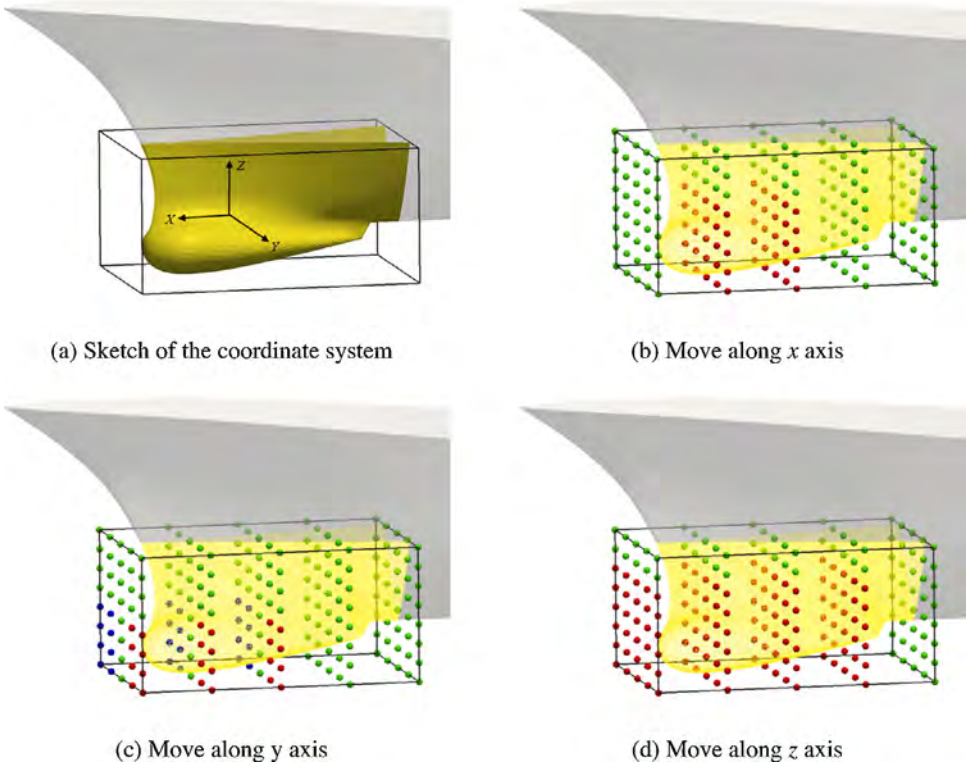

(a) Sketch of the coordinate system

(b) Move along x axis

(c) Move along y axis

(d) Move along z axis

Fig. 8. Point sets to be moved in FFD method.

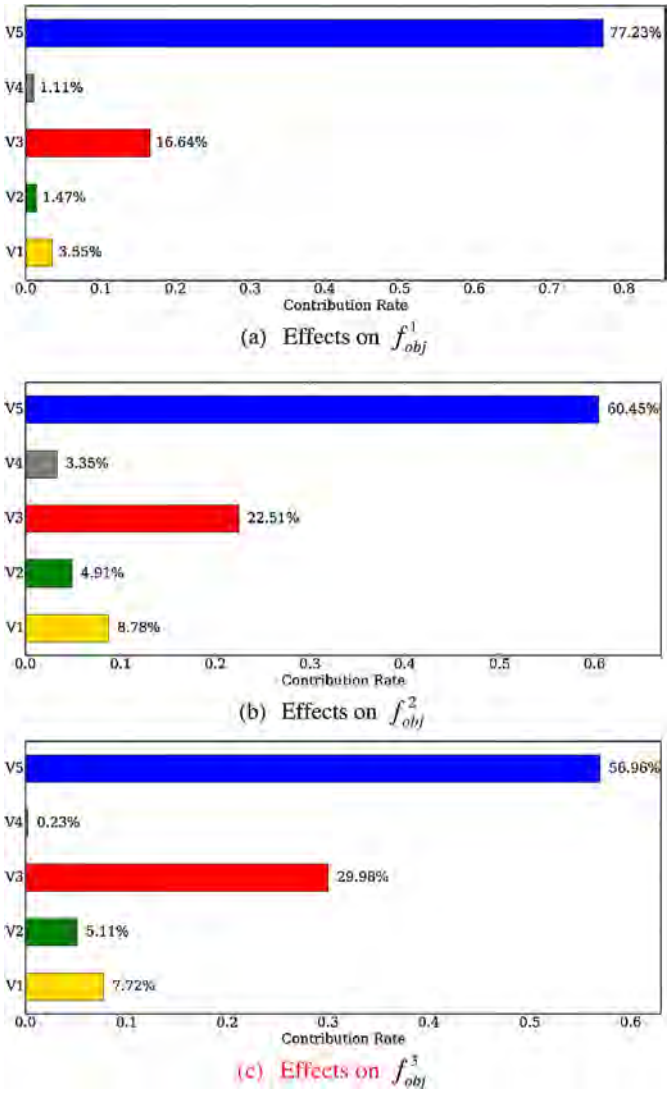

Fig. 9. Results of ANOVA test.

4.3. Optimization algorithm

NSGA and NSGA-II are proposed by Srinivas and Deb [30]. They have been applied into many engineering optimization problems. In this paper, NSGA-II algorithm is adopted to drive the optimization procedure, which should be verified first for its effectiveness and logic. The objective function proposed by Deb et al. [31] is used to verify the effectiveness of NSGA-II algorithm:

$$\min f_1(x) = x_1 \tag{12}$$

$$\min f_2(x) = g \times h \tag{13}$$

$$g = 1 + 10 \times (n-1) + \sum_{i=2}^{n} \left(x_i^2 - 10 \times \cos(4\pi x_i)\right) \tag{14}$$

$$h = 1 - \sqrt{f_1(x)/g} \tag{15}$$

$$0 \le x_1 \le 1, -5 \le x_{2,\ldots,n} \le 5 \tag{16}$$

After 20000 iterations of 100 generations and 200 individuals, the Pareto-optimal solutions are obtained as shown in Fig. 6. The Pareto front is plump and represents the optimal solutions. It shows that the optimization based on NSGA-II is reasonable and effective.

Table 1
Total resistance coefficients ($\times 10^{-3}$) predicted by three methods and comparisons.

Fr	0.21	0.28	0.35
[1] NM[a]	4.223	4.276	4.567
[2]naoe-FOAM-SJTU	3.941	4.283	4.770
[3] EFD	3.950	4.230	4.840
[1]-[2]	7.14%	−0.16%	−4.24%
[1]–[3]	6.90%	1.09%	−5.63%
[2]-[3]	−0.22%	1.26%	−1.46%

[a] The sum of the friction drag C_f given by ITTC formula and the wave drag C_w predicted by NM theory is used as the total drag.

5. Definition of the optimization problem

5.1. Initial design

The initial design is DTMB Model 5415, which was conceived as a preliminary design for a Navy surface combatant. The hull geometry includes both a sonar dome and transom stern. A large amount of experimental results are available in [25] provided by an international cooperative project between INSEAN, IIHR and DTMB. The geometry of the initial model is presented in Fig. 7.

Total resistance of the initial design at Fr = 0.21, 0.28, 0.41 are evaluated using the NM theory and ITTC formula to validate this simulation tool. Results are shown in Table 1 and compared against experimental measurements from [25] and the computational results from naoe-FOAM-SJTU [32]. The comparisons of total resistance coefficients show acceptable agreement between NM, CFD and EFD.

5.2. Objective functions, design variables and geometrical constraints

The aim of the present study is to develop the optimal hull forms with minimum total resistance at specific speeds (Fr = 0.21, 0.28, 0.35). The optimal hull forms determined by single objective optimization always result in a large drag reduction within a narrow range including the speed while a large drag increase at off-design speeds compared with the initial one [1], so three total resistance coefficients at discrete speeds are used as objective functions in this problem to avoid awkward optimization design as mentioned above:

$$f_{obj}^1 = C_w + C_f, atFr = 0.21 \tag{17a}$$

$$f_{obj}^2 = C_w + C_f, atFr = 0.28 \tag{17b}$$

$$f_{obj}^3 = C_w + C_f, atFr = 0.35 \tag{17c}$$

where C_w is wave drag coefficient predicted by NM theory and varies with the changing hull forms, while C_f is friction drag coefficient given by ITTC formula. It is notable that C_f is actually constant during the optimization process since the length of ship remains unchanged.

As previously stated, two approaches, shifting method and FFD method, are employed to modify the geometry of hull form globally and locally respectively. Specifically, both of the fore- and aft-body are modified by two shape functions in shifting method. The two parameters (entrance angle α_{1f}, run angle α_{1a}) are used as the design variables while the others involved in shifting method are fixed in value ($x_{1f} = 0, x_{2f} = 0.56, x_{1a} = -0.5, x_{2a} = 0, \alpha_{2f} = 0.26, \alpha_{2a} = -0.25$). With regard to FFD method, 200 control points are imposed in a parallelepiped which contains the sonar dome. For modifying the shape of sonar dome, three sets of control points are chosen to move along the x, y, z axes respectively while the amount of movements is decided by corresponding design variables. The three point sets are illustrated in Fig. 8 where the green points are

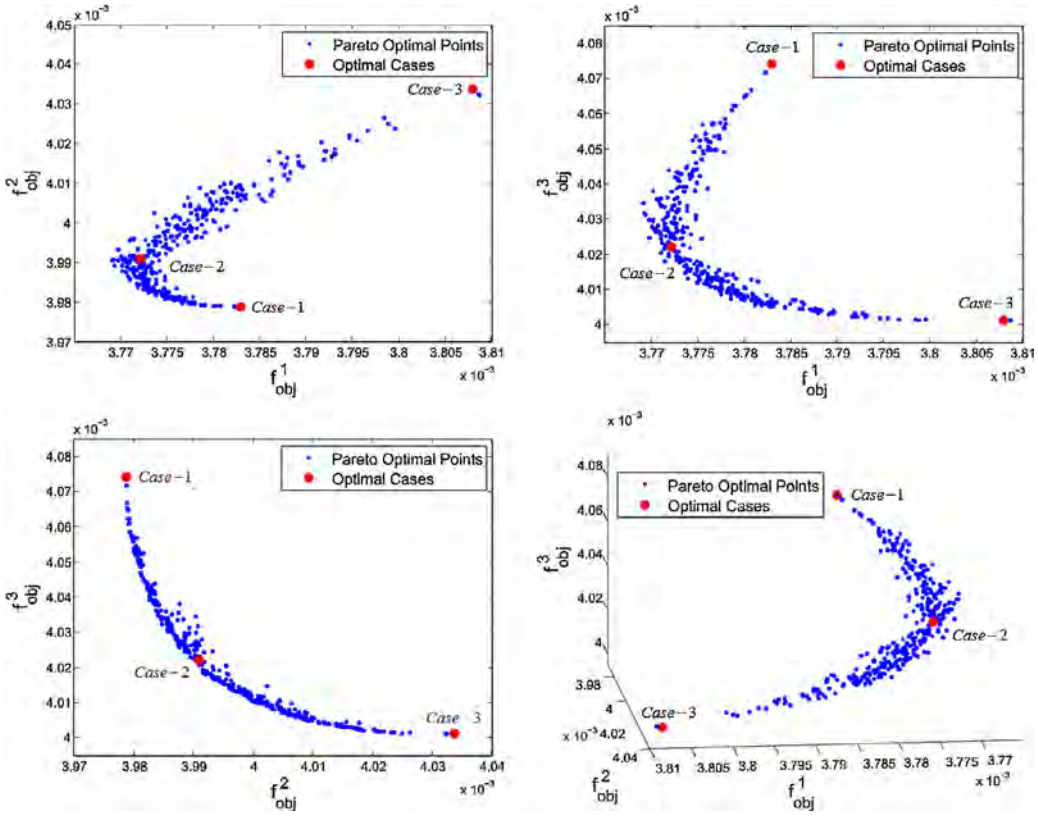

Fig. 10. Pareto optimal points and optimal cases in objective functions space.

fixed and the red points are moved along specific direction. Specifically, the blue and red points in Fig. 8(c) should move in opposite direction with same distance to keep the geometrical symmetry of ship bow.

Additionally, some geometric constraints are imposed on the design variables, the displacement (∇), the wetted surface area (S_{wet}) and the principal dimensions of the ship. Detail information regarding these constraints is reported in Table 3.

5.3. Experimental design method, approximation model and optimizer

Based on the optimal Latin hypercube design method mentioned earlier, a series of 100 sample points with five design variables α_{1f} (entrance angle), α_{1a} (run angle), Δx(displacement of control points in x direction), Δy (displacement of control points in y direction), Δz (displacement of control points in z direction) are generated, then the computations are performed with NM theory and ITTC formula to obtain the corresponding total resistance coefficients.

Moreover, the ANOVA test is performed to represent the influence of each design variable on the objective functions. The results are explored and presented in Fig. 9, where the five design variables (α_{1f}, α_{1a}, Δx, Δy,Δz) are represent as V1–V5. It is obviously from Fig. 9 that the impacts of variables on different objective functions vary widely. Main effects are always from V5(Δz) and V3(Δx), but the total influence of the others is not ignorable, and the computational cost involved five design variables is adequately affordable, thus, all of these five design variables are adopted in optimization.

In order to represent the relationship between the input (design variables) and the output (resistance coefficients at specific speeds), kriging model is served as an approximation model in present work. An error analysis is carried out to check the approximation capability of these kriging models in terms of the sample points. The results including the maximum absolute error, the average absolute error and the root mean square error (MSE) are listed in Table 2. It can be concluded that the kriging models are effective to approximate the objective functions in design space.

Table 2
Error analysis for kriging model.

	Model-1	Model-2	Model-3
Max ABS(error) ($\times 10^{-4}$)	0.961	0.693	0.812
Avg ABS(error) ($\times 10^{-4}$)	0.367	0.310	0.295
root MSE ($\times 10^{-4}$)	0.693	0.345	0.344

As for optimizer, a muti-objective genetic algorithm named NSGA-II is adopted to provide a set of optimal solutions using pareto-optimal front. In the optimization procedure, the number of generations is set as 300 while the size of population is 200, thus, 200 × 300 individuals will be generated and evaluated before the final results of optimization are obtained. A complete definition of this problem is reported in Table 3.

6. Results and validation

6.1. Optimization results

The pareto optimal set is constructed based on the populations generated in optimization process, and these non-dominated solutions which conform the concept of pareto optimality are shown in Fig. 10, where each blue point represents an optimal solution while three typical examples are marked in red to be analyzed further. The relationship with highly nonlinear between any pair of objective functions is revealed in Fig. 10. Especially, an obvious trade-off can be observed between f^2_{obj} (drag at middle speed) and f^3_{obj} (drag at higher speed), while more uncertain relationship are existed inf^2_{obj}

Table 3
Definition of the optimization problem.

Type		Definition	Note
Initial hull		DTMB Model 5415	
Objective functions		$f^1_{obj} = C_w + C_f, atFr = 0.21$ $f^2_{obj} = C_w + C_f, atFr = 0.28$ $f^3_{obj} = C_w + C_f, atFr = 0.35$	Bare hull Aim is to search for hull forms with possible drag reduction at given speeds
Design variables			
α_{1f}	(Variable1)	[−0.015, 0.015]	Entrance angle
α_{1a}	(Variable2)	[−0.015, 0.015]	Run angle
Δx	(Variable3)	[−0.012, 0.012]	Displacement in x direction
Δy	(Variable4)	[−0.006, 0.006]	Displacement in y direction
Δz	(Variable5)	[−0.015, 0.015]	Displacement in z direction
Geometric constraints			
Main dimensions		L_{pp}, D, B are fixed	
Displacement (∇)		Maximum variation ±1%	
Wetted surface area (S_{wet})		Maximum variation ±1%	
Experimental design		OLHS method	Generate 100 sample points
Approximation model		Kriging model	
Optimizer		NSGA-II	
Size of population		200	
Number of generations		300	

Table 4
Summary of the prediction results for initial and optimal hulls based on NM theory.

Fr		0.21			0.28			0.35		
Components		$C_w(\times10^{-3})$	$C_f(\times10^{-3})$	$C_t(\times10^{-3})$	$C_w(\times10^{-3})$	$C_f(\times10^{-3})$	$C_t(\times10^{-3})$	$C_w(\times10^{-3})$	$C_f(\times10^{-3})$	$C_t(\times10^{-3})$
Initial	Coeff.	1.162	3.060	4.223	1.365	2.911	4.276	1.709	2.803	4.513
Case-1	Coeff.	0.797	3.060	3.857	1.138	2.911	4.049	1.350	2.803	4.153
	Reduction	/	/	8.66%	/	/	5.30%	/	/	7.96%
Case-2	Coeff.	0.795	3.060	3.855	1.159	2.911	4.070	1.312	2.803	4.116
	Reduction	/	/	8.71%	/	/	4.83%	/	/	8.80%
Case-3	Coeff.	0.831	3.060	3.891	1.175	2.911	4.086	1.274	2.803	4.077
	Reduction	/	/	7.86%	/	/	4.45%	/	/	9.65%

(drag at middle speed) and f^1_{obj} (drag at lower speed), f^3_{obj} (drag at higher speed) and f^1_{obj} (drag at lower speed) respectively.

The pareto optimal set provides over 5000 solutions with drag reductions in different degree at three given speeds. In order to verify these optimization results, three typical optimal hull forms denoted as *Case-1*, *Case-2* and *Case-3* are chosen for further analysis. Comparisons of 3D models between the initial design and the optimal ones are shown in Fig. 11, and the buttock lines colored with horizontal distance are also plotted on 3D models to present the geometrical differences distinctly. Also, more details of the comparisons given by body plans are illustrated in Fig. 12.

It can be observed from Fig. 11 that all the three optimal hull forms display some geometric similarities. For the local modification controlled by FFD method in Fig. 12, the widths of domes significantly decrease by about 35% in *Case-2*, and about 30% in *Case-1* and *Case-3*, while the lengths of domes are slightly reduced as well. The depths of domes in *Case-1* and *Case-3* both increase, but a small reduction can be observed in *Case-2*, which proves that the variation of Δz (V5) has less impact on the objective functions once again. As for the global modification carried out by shifting method in Fig. 13, the volume distribution is moved backward for the aft body and forward for the front body. It means that the surfaces around bow and stern tend to be full and the midship parts tend to be slender. Moreover, all of the geometric constraints have been satisfied in the three cases. Main dimensions are fixed during the optimization process, and the variations of displacement and wetted surface are less than 1% as shown in Fig. 11. It is critical to maintaining the availability of optimal ships by enforcing constraints conditions on the optimization problem. It also can be found that all the wetted areas of the three optimal cases become smaller, in other words, the decreases of drag coefficients

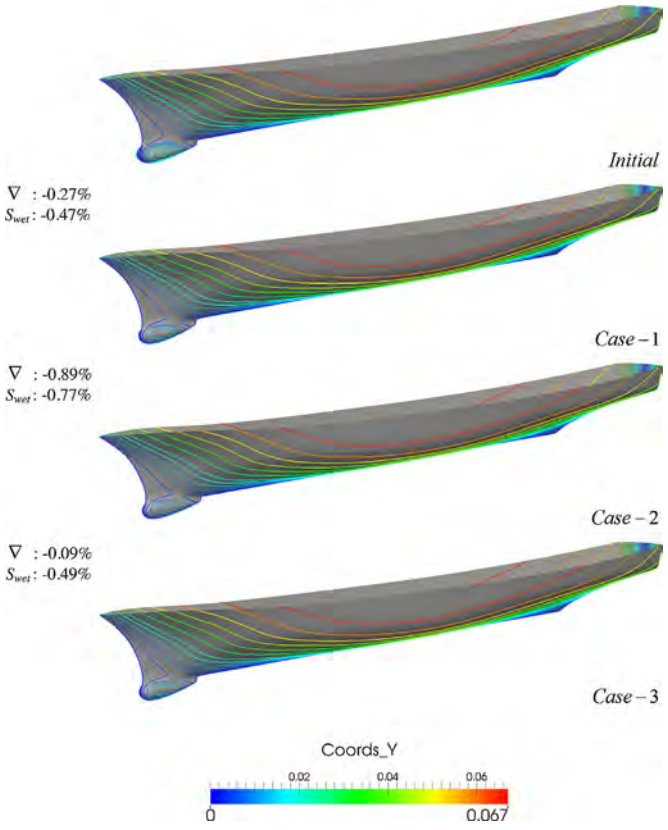

Fig. 11. Comparisons of 3D models between the initial design and the optimal hull forms.

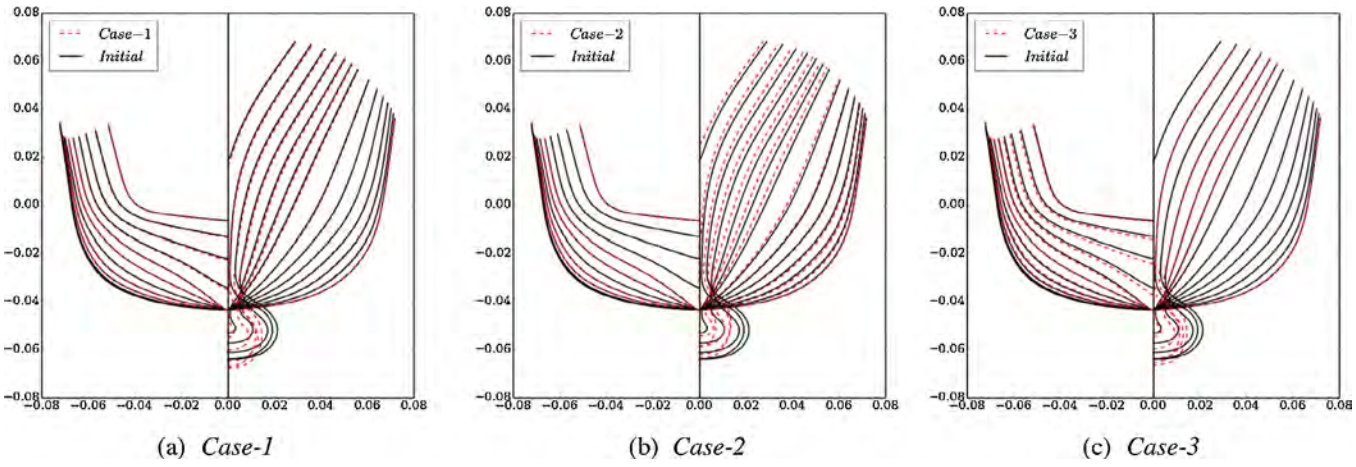

Fig. 12. Comparisons of transverse cross-section plans between the initial design and the optimal hull forms.

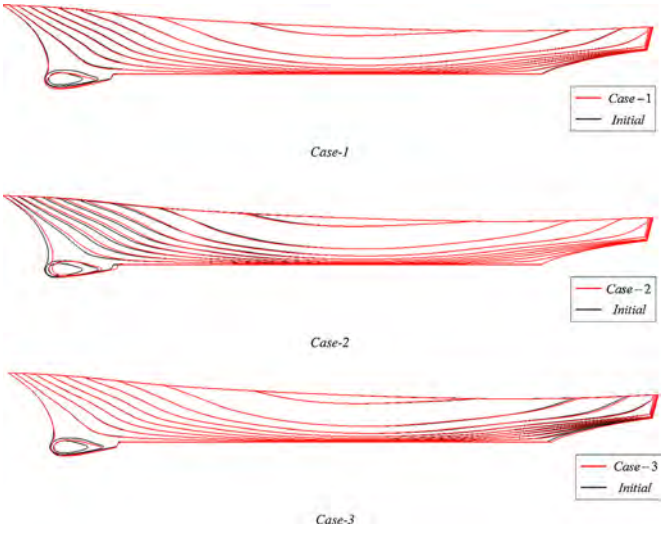

Fig. 13. Comparisons of longitudinal cross-section plan between the initial design and the optimal hull forms.

are caused by the changes of hull forms rather than the variations of wetted areas.

6.2. Validation with NM theory

To assess the validity of the optimization case based on approximation technique, NM theory is employed to analyze the resistance performances of the optimal hulls.

The summary of the prediction results provided by NM theory is summarized in Table 4. As mentioned above, total resistance coefficient can be simplified as the sum of wave drag coefficient C_w and friction drag coefficient C_f, while the former is predicted by NM theory and the latter is given by ITTC formula. Based on this simplification, all of the drag reduction comes from the decrease of wave component due to the fact that the main dimensions are fixed so the friction drag coefficient C_f keeps unchanged during the present optimization procedure.

As shown in Table 4, the results indicate significant reductions in values of objective functions (total resistance coefficients), i.e., those for *Case-1* are 8.66%, 5.30% and 7.96%; those for *Case-2* are 8.71%, 4.83% and 8.80% respectively; and those for *Case-3* are 7.86%, 4.45% and 9.65%. In order to further demonstrate these optimization results, postprocessings for *Case-2* and initial hull are performed and compared with each other. Fig. 14 depicts the wave patterns (non-dimensionalised by ship length) generated by the initial hull (upper) and the optimal hull, *Case-2* (lower). Fig. 15 illustrates the comparisons of dimensionless wave profiles where the blue solid lines represent the original hull and the orange dashed lines represent *Case-2*, specially, results from an experimental campaign (green dots) are also plotted here. Fig. 16 displays the pressure distributions on the underwater part of the domes for both initial (upper) and optimal (lower) hulls. It is notable that all these data based on NM theory are corresponding to the ship model with total length of 5.72m, just as the one adopted in previous experiments of INSEAN.

The improvement of the resistance performance is reflected in Figs. 14–16. The amplitudes of the optimal hull generated waves are clearly lower than the ones generated by initial hull, and this phenomenon can be observed more obviously in the stern waves. Lower amplitudes indicate the loss reduction of the wave energy, and the drag performance will improve in terms of the conservation law of energy. The optimal dome with slender shape leads to smaller bow waves and smoother first trough which are illustrated in Fig. 15 and also can be detected near the bow region in Fig. 14, and they are always regards as clear indications of a reduced wave component of the total resistance [9]. The same conclusion is confirmed in Fig. 16. Both of the positive and negative pressures are effectively reduced on the optimal dome surface, which is favorable to the diminution of pressure drag.

The total and wave drag coefficients in a wide range of speed including the three optimization design points are computed with NM theory and summarized in Fig. 17. It should be noted that the reduction of total drag and wave components is achieved in the whole speed range for the three cases. The resistance curves of *Case-1* and *Case-3* are found to be identical due to the geometric similarity between the two optimal designs while *Case-2* has more improvements of drag performance at low and high speeds.

6.3. Validation with naoe-FOAM-SJTU solver

To provide more accurate validation of the optimal solutions considering realistic viscous effect, naoe-FOAM-SJTU solver, a high-fidelity tool based on RANS flow equation is used for prediction, and the numerical results are summarized in Table 5.

Table 5 shows the numerical predictions of total resistance and the corresponding reductions for initial and optimal hulls. It can be found that the reductions listed in Table 5 are less than those given in Table 4 while the ranking is still unchanged under the same speed. The basic cause for the results may lie in the limitations of the simulation tool (NM theory) used in optimization process.

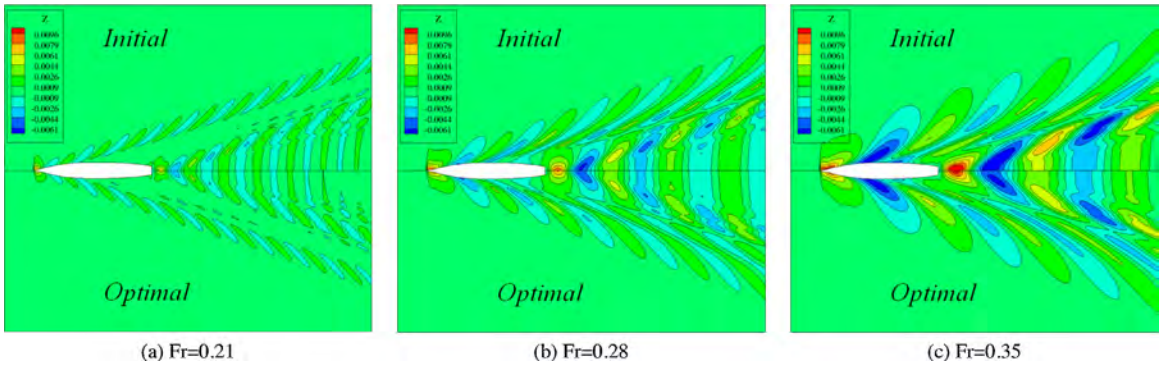

Fig. 14. Comparison of the wave patterns between initial and optimal hulls computed with NM theory.

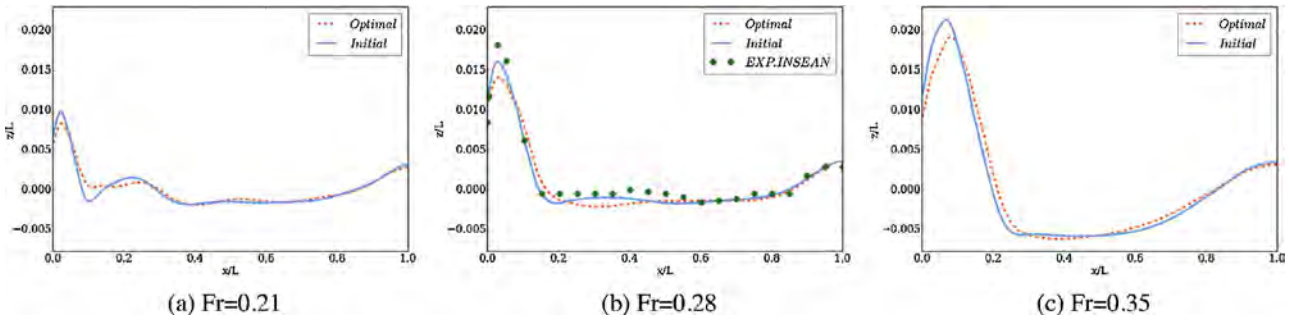

Fig. 15. Comparison of the wave profiles between initial and optimal hulls computed with NM theory.

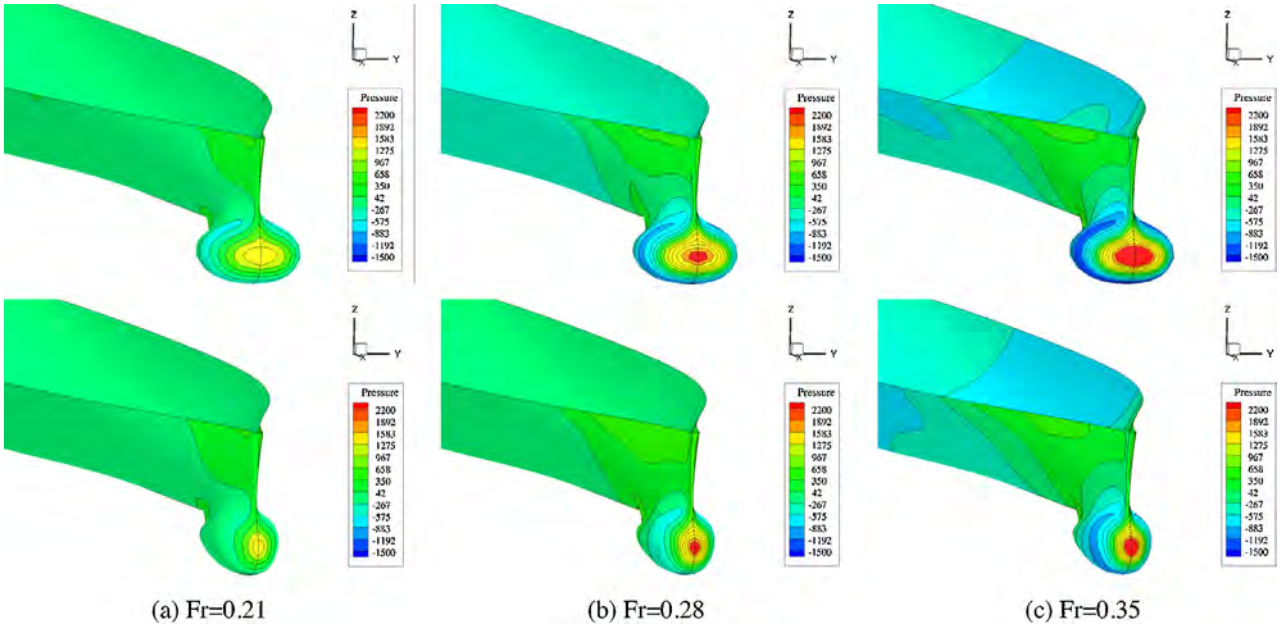

Fig. 16. Comparison of the pressure distribution between initial and optimal hulls computed with NM theory.

Table 5
Summary of the prediction results for initial and optimal hulls based on naoe-FOAM-SJTU solver.

Fr		0.21			0.28			0.35		
	$S_{wet}(m^2)$	F_t (N)	C_t ($\times 10^{-3}$)	Reduction	F_t (N)	C_t ($\times 10^{-3}$)	Reduction	F_t (N)	C_t ($\times 10^{-3}$)	Reduction
Initial	2.43046	11.84	3.941	/	22.88	4.283	/	39.80	4.770	/
Case-1	2.41922	11.30	3.779	4.12%	21.89	4.118	3.85%	39.25	4.725	0.93%
Case-2	2.39298	11.09	3.749	4.87%	21.85	4.156	2.96%	38.41	4.675	1.99%
Case-3	2.41872	11.44	3.827	2.91%	22.12	4.162	2.83%	38.67	4.656	2.37%

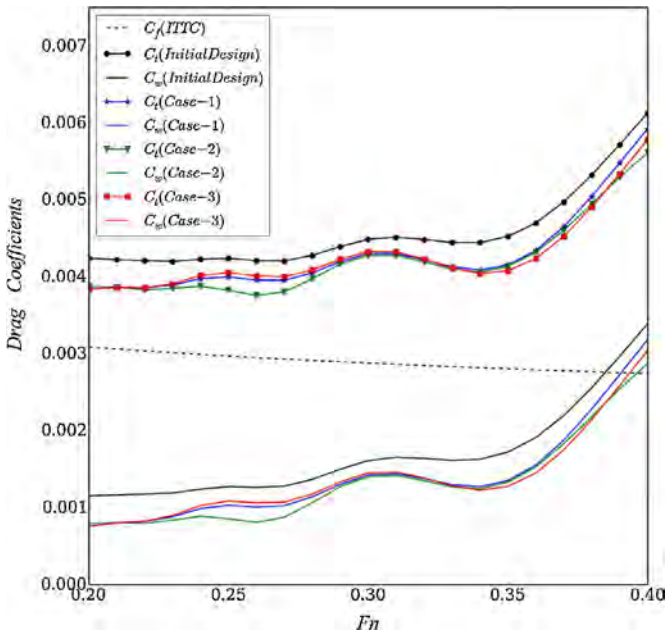

Fig. 17. Comparisons of total and wave drag coefficients in a wide range of speed between initial design and optimal designs.

It is well known that wave-drag predictions based on analytical method always exhibit unrealistic large oscillations with respect to ship speeds [12]. Therefore, the solutions with "unrealistic" drag reductions will be obtained by using the optimizer and NM-based kriging model. However, although the predictions associated with NM theory are not accurate enough for many applications especially in the late stage of design, it is being able to provide correct relative comparisons of the drags of alternative solutions, which guarantees the accuracy of ranking and the availability of the NM theory in optimization.

Then, the postprocessings for *Case-2* and initial hull are performed using the results evaluated by naoe-FOAM-SJTU, and the length of ship is set as 5.72 m for the same reason as mentioned above. Fig. 18 shows the comparisons of wave patterns between initial and optimal designs, and the free surface is non-dimensionalised with ship length. The overall wave field is shown on the left, while the close-up views of bow and stern are placed on the upper-right and lower-right sides. The dimensionless wave profiles along the original (blue solid lines) and optimal (orange dashed lines) hulls at different speeds are given and compared in Fig. 19, and the experimental measurements (green points) are provided by [25]. Finally, Fig. 20 displays the pressure distributions on the bows and sonar domes for both initial (upper) and optimal (lower) hulls.

More realistic field is illustrated in Figs. 18–20 based on the high-fidelity simulation tool. The aforementioned feature related to drag reduction can be observed in these figures as well. Wave amplitudes associated with the optimal hull are reduced evidently in the overall field with respect to the initial one, in particular, the steepness of bow wave and the first trough around the bow region are smoothed, and the location of the first bow wave is shifted backwards according to Fig. 19. Additionally, the size of the region of maximum pressure values is lower while the pressure gradients are reduced remarkably on optimal bow surface. All these features clearly contribute to the reduction of wave resistance and are consistent with the aforementioned ones provided by NM-based validation.

7. Conclusions

A numerical multi-objective optimization tool, OPTShip-SJTU, has been developed and tested in present work. The surface combatant DTMB Model 5415 is adopted as initial hull form, and the aim is to search for optimal hull forms with improved resistance performances at three given speeds (Fr = 0.21, 0.28, 0.35). During the procedure of optimization, the region of bow and sonar dome is deformed with free-form deformation (FFD) method and the global surface is modified by shifting method. Both of the modification techniques are sufficiently flexible to generate a series of realistic alternative hull forms with a few number of design variables involved. A practical simulation tool based on the Neumann-Michell (NM) theory is implemented in the hydrodynamic performance evaluation module to predict the wave drag.

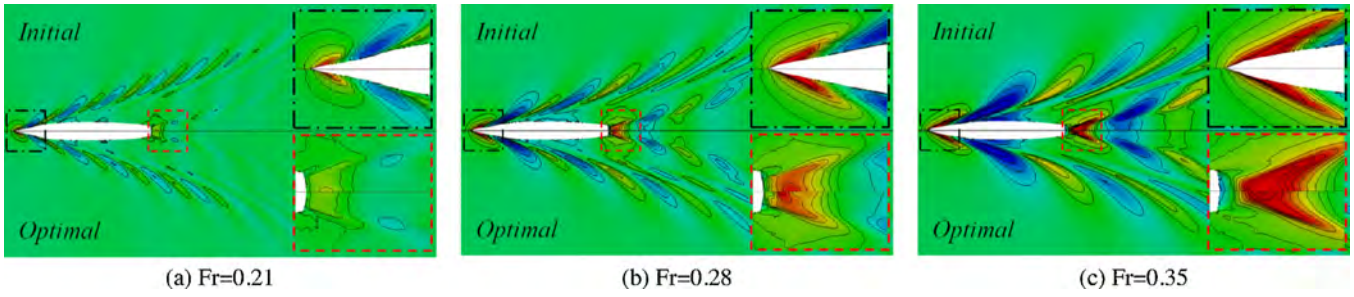

Fig. 18. Comparison of the wave patterns between initial and optimal hulls computed with naoe-FOAM-SJTU.

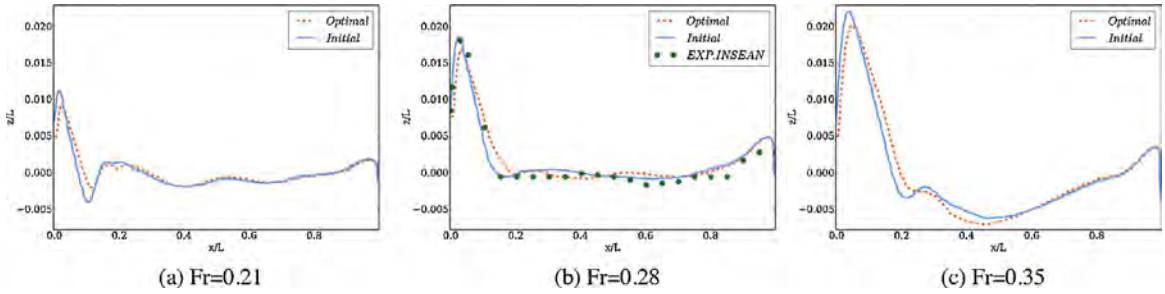

Fig. 19. Comparison of the wave profiles between initial and optimal hulls computed with naoe-FOAM-SJTU.

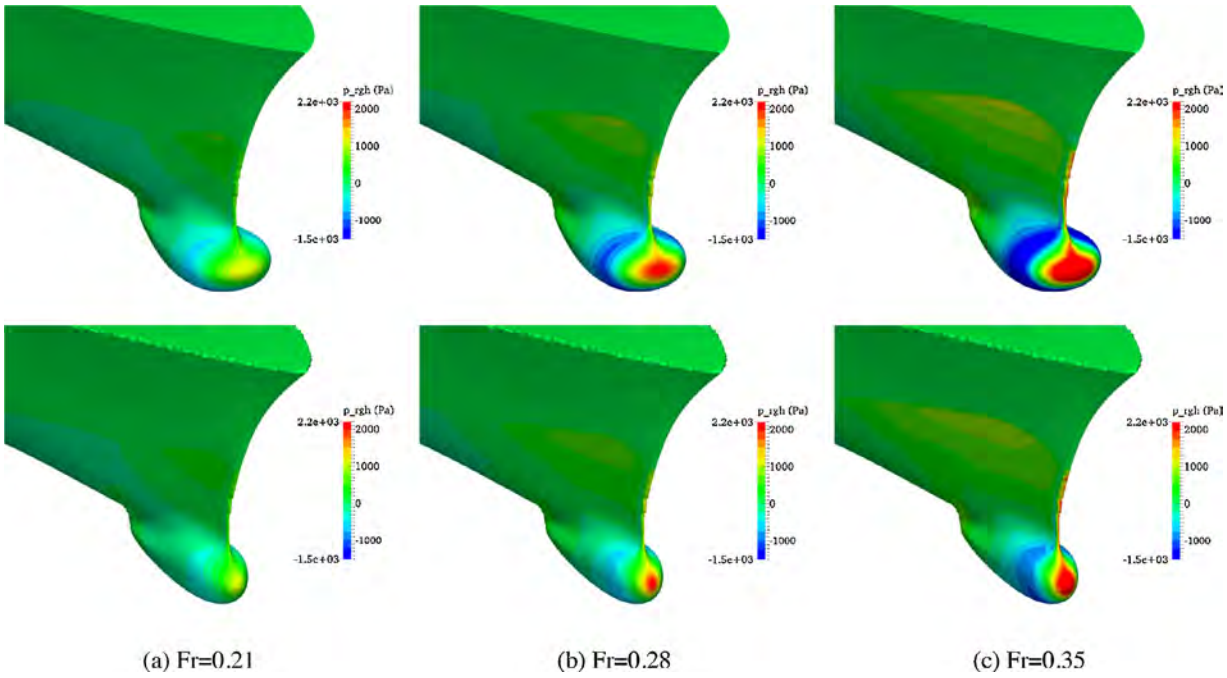

Fig. 20. Comparison of the wave profiles between initial and optimal hulls computed with naoe-FOAM-SJTU.

Optimized Latin hypercube sampling (OLHS) method and kriging model have been employed here to establish the relationship between the objective functions and the design variables, and the computational effort in optimization process has decreased remarkably as expected. Besides, the analysis of variance (ANOVA) method also has been introduced to represent the influence of each design variables on the objective functions. The optimizer is based on a muti-objective genetic algorithm, NSGA-II, and pareto-optimal front is obtained eventually.

The pareto optimal set provides over 5000 solutions with drag reductions in different degree, and three typical optimal hull forms denoted as *Case-1*, *Case-2* and *Case-3* are chosen from it for further analysis. Two simulation tools, which are NM theory and RANS-based CFD solver naoe-FOAM-SJTU, have been employed to confirm the improvements of resistance performances for these optimal hulls. Numerical results indicate that the reduction in total resistance coefficients has been achieved for all cases at given speeds, and the clear reduction of wave-making resistance can be observed from the comparisons of fields generated by initial and optimal hulls.

The future work will focus on integrating various evaluation tools for overall hydrodynamics performances into the optimization tool OPTShip-SJTU. Multidisciplinary design optimization of hull form can result in better optimal designs with higher practicality and reliability.

Acknowledgements

This work was supported by the National Natural Science Foundation of China (Grant Nos. 11072154, 51379125, 51109132), the National Key Basic Research Development Plan (973 Plan) Project of China (Grant No. 2013CB036103), High Technology of Marine Research Project of the Ministry of Industry and Information Technology of China, the Program for Professor of Special Appointment (Eastern Scholar) at Shanghai Institutions of Higher Learning (Grant No. 2013022), the Specialized Research Fund for the Doctoral Program of Higher Education of China (Grant No. 20110073120015), and the Center for HPC of Shanghai Jiao Tong University, to which the authors are most grateful.

References

[1] H. Kim, Multi-objective Optimization for Ship Hull Form Design. Ph.D. Thesis, George Mason University, USA, 2009.
[2] D. Peri, M. Rossetti, E.F. Campana, Design optimization of ship hulls via CFD techniques, J. Ship Res. 45 (2) (2001) 140–149.
[3] Y. Tahara, M. Diez, S. Volpi, X. Chen, E.F. Campana, F. Stern, CFD-based multiobjective stochastic optimization of a waterjet prepelled high speed ship, in: 30th Symposium on Naval Hydrodynamics, Hobart, Tasmania, Australia, 2014.
[4] K. Suzuki, H. Kai, S. Kashiwabara, Studies on the optimization of stern hull form based on a potential flow solver, J. Mar. Sci. Technol. 10 (2) (2005) 61–69.
[5] J.L. Hess, A.M.O. Smith, Calculation of non-lifting potential flow about arbitrary three-dimensional bodies, J. Ship Res. 8 (2) (1964) 22–44.
[6] C.W. Dawson, A practical computer method for solving ship-wave problems, in: 2nd International Conference on Numerical Ship Hydrodynamics, Berkeley, USA, 1977.
[7] B.J. Zhang, Research on optimization of hull lines for minimum resistance based on Rankine source method, J. Mar. Sci. Technol. 20 (1) (2012) 89–94.
[8] S. Percival, D. Hendrix, F. Noblesse, Hydrodynamic optimization of ship hull forms, Appl. Ocean Res. 23 (2001) 337–355.
[9] E.F. Campana, D. Peri, Y. Tahara, F. Stern, Shape optimization in ship hydrodynamics using computational fluid dynamics, Comput. Methods Appl. Mech. Eng. 196 (1–3) (2006) 634–651.
[10] H. Tahara, D. Peri, E.F. Campana, F. Stern, Computational fluid dynamics-based multiobjective optimization of a surface combatant using a global optimization method, J. Mar. Sci. Technol. 13 (2) (2008) 95–116.
[11] W. Wilson, D. Hendrix, J. Gorski, Hull form optimization for early stage ship design, Nav. Eng. J. 122 (2) (2010) 53–65.
[12] F. Noblesse, F.X. Huang, C. Yang, The Neumann-Michell theory of ship waves, J. Eng. Math. 79 (1) (2013) 51–71.
[13] C. Yang, F.X. Huang, Practical evaluation of the drag of a ship for design and optimization, J. Hydrodyn. 25 (5) (2013) 645–654.
[14] H. Kim, C. Yang, H. Kim, H.H. Chun, Hydrodynamic optimization of a modern container ship using variable fidelity models, in: 19th International Offshore and Polar Engineering Conference, Osaka, Japan, 2009.
[15] M. Diez, E.F. Campana, F. Stern, Design-space dimensionality reduction in shape optimization by Karhunen–Loève expansion, Comput. Methods Appl. Mech. Eng. 283 (283) (2015) 1525–1544.
[16] H. Kim, S. Jeong, C. Yang, F. Noblesse, Hull form design exploration based on response surface method, in: 21 St International Offshore and Polar Engineering Conference, Maui, Hawaii, USA, 2011.

[17] Y. Tahara, D. Peri, E.F. Campana, F. Stern, Single-and multi-objective design optimization of a fast multihull ship: numerical and experimental results, J. Mar. Sci. Technol. 16 (4) (2011) 412–433.
[18] Y. Tahara, E.G. Paterson, F. Stern, Y. Himeno, Flow-and wave-field optimization of surface combatants using CFD-based optimization methods, in: 23rd ONR Symposium on Naval Hydrodynamics, Val De Reuil, France, 2000.
[19] A. Pinto, D. Peri, E.F. Campana, Multiobjective optimization of a containership using deterministic particle swarm optimization, J. Ship Res. 51 (3) (2007) 217–228.
[20] Z.R. Shen, D.C. Wan, RANS computations of added resistance and motions of a ship in head waves, Int. J. Offshore Polar Eng. 23 (04) (2013) 263–271.
[21] T.W. Sederberg, S.R. Parry, Free-form deformation of solid geometric models, ACM Siggraph Comput. Graphics 20 (4) (1986) 151–160.
[22] D. Peri, E.F. Campana, Simulation based design of fast multi-hull ship, in: 26th Symposium on Naval Hydrodynamics, Rome, Italy, 2006.
[23] H. Kim, C. Yang, F. Noblesse, Application of a practical multi-objective optimization tool to hydrodynamic design of a surface combatant ship, in: Grand Challenges in Modeling & Simulation Conference, Istanbul, Turkey, 2009.
[24] H. Kim, C. Yang, Design optimization of bulbous bow and stern end bulb for reduced drag, in: 23rd International Offshore and Polar Engineering Conference, Anchorage, Alaska, USA, 2013.
[25] A. Olivieri, F. Pistani, A. Avanzini, F. Stern, R. Penna, Towing tank experiments of resistance, sinkage and trim, boundary layer, wake, and free surface flow around a naval combatant INSEAN 2340 model. No. IIHR-TR-421. IOWA UNIV IOWA CITY COLL OF ENGINEERING, 2001.
[26] T.W. Simpson, Comparison of Response Surface and Kriging Models in the Multidisciplinary Design of an Aerospike Nozzle. NASA/CR-1998-206935, Institute for Computer Applications in Science and Engineering, NASA Langley Research Center, 1998.
[27] T.W. Simpson, T.M. Mauery, J.J. Korte, F. Mistree, Kriging models for global approximation in simulation-based multidisciplinary design optimization, AIAA J. 39 (12) (2001) 2233–2241.
[28] R. Jin, W. Chen, A. Sudjianto, An efficient algorithm for constructing optimal design of computer experiments, J. Stat. Plann. Inference 134 (1) (2005) 268–287.
[29] M. Zhao, W.C. Cui, Application of the optimal Latin hypercube design and radial basis function network to collaborative optimization, J. Mar. Sci. Appl. 6 (3) (2007) 24–32.
[30] N. Srinivas, K. Deb, Muiltiobjective optimization using nondominated sorting in genetic algorithms, J. Evol. Comput. 2 (3) (1994) 221–248.
[31] K. Deb, S. Agrawal, A. Pratap, T. Meyarivan, A fast elitist non-dominated sorting genetic algorithm for multi-objective optimization: NSGA-II. Conference on ParallelProblem Solving from Nature (PPSN VI). 1917, Springer, 2000, pp. 849–858.
[32] Z.R. Shen, L. Jiang, S. Miao, D.C. Wan, C. Yang, RANS simulations of benchmark ships based on open source code, in: 7th International Workshop on Ship Hydrodynamics (IWSH'2011), Shanghai, China, 2011.